Journal of Hazardous Materials 164 (2009) 204–214

Contents lists available at ScienceDirect

Journal of Hazardous Materials

journal homepage: www.elsevier.com/locate/jhazmat

A model and experimental study for dissolution efficiency of gaseous substrates through in situ sparging

K.F. Liang, M.C. Tom Kuo*

Department of Mineral and Petroleum Engineering, National Cheng Kung University, Tainan, Taiwan

ARTICLE INFO

Article history:
Received 25 March 2008
Received in revised form 30 July 2008
Accepted 31 July 2008
Available online 22 August 2008

Keywords:
Dissolution
In situ sparging
Toluene

ABSTRACT

Delivering electron acceptors, electron donors, and nutrients in gas state has been practiced for in situ bioremediation. A mathematical model based on air-channel concept was developed in this paper to assess the dissolution transient behavior of gaseous substrates for an in situ sparging process using their chemical and physical properties, aquifer-media characteristics, and field operating conditions. Using toluene as an example, the model was verified with experimental data obtained at field sparging rates ranging from 40 to 80 L air/min. The verified model is a useful means of predicting the dissolution behavior of gaseous substrates during sparging in an unconfined aquifer.

1. Introduction

Delivering electron acceptors, electron donors, and nutrients in gas state has been practiced for in situ bioremediation. A model and experimental study of dissolution efficiency and rate of gaseous substrates in groundwater can be useful for design work and performance evaluation of in situ bioremediation. In situ air sparging and biosparging [1–4] are most widely used remedial techniques by which contaminants are removed from groundwater through volatilization and aerobic biodegradation. Providing an adequate quantity of electron acceptor (e.g., oxygen) is the most critical requirement for in situ aerobic bioremediation. Delivering electron acceptors (air), electron donors (methane and propane), and nutrients (nitrous oxide and triethyl phosphate) in gas state has also been applied for in situ aerobic cometabolism of TCE-contaminated sites to feed methane-utilizing-bacteria [5–10] and propane-utilizing-bacteria [10,11]. Direct hydrogen sparging is another potential application for sites contaminated with PCE or TCE [12,13].

The efficiency of in situ bioremediation observed in the field is often lower than that observed in laboratories [14–16]. One of the major reasons is due to the contact efficiency for air, substrates, and bacteria in the field are lower than that obtained in laboratories. Delivering substrates in gas state instead of liquid state can enhance the contact and sweep efficiency of electron acceptors, electron donors, and nutrients within the contaminated subsurface aquifers. This can be illustrated by two field studies of cometabolic transformations of TCE by aerobic microorganisms growing on toluene [15,17]. McCarty et al. [15] demonstrated at full scale in situ cometabolic degradation of TCE in groundwater through toluene injection. Oxygen or hydrogen peroxide was mixed with neat toluene in water at the surface and the solution was injected into the subsurface. Well workover service to remove excessive microbial growth was one major operational cost of the in situ bioremediation [15]. Kuo et al. [17] conducted in situ pilot studies of aerobic cometabolism to evaluate the injection of toluene-vapor and air into TCE-contaminated aquifer. Delivery of primary substrate (toluene) in a vapor state with air enhanced the growth of indigenous toluene-utilizing bacteria that would degrade TCE by aerobic cometabolism. Meanwhile, delivering toluene in a vapor state effectively reduced potential clogging near the injection points due to excessive microbial growth, which was observed in the field when the injection of neat toluene was employed. Mathematical modeling and experimental data are useful for quantifying the dissolution efficiency and transport rate of toluene-vapor during in situ air sparging.

To evaluate the dissolution efficiency of gaseous substrates in groundwater, it is commonly assumed that the air and water concentrations are in local equilibrium. Models are also available in the literature for predicting the dissolution transient behavior of oxygen during in situ sparging [1–3]. Johnson [1] developed an analytical model to understand the rate of oxygen transport during in situ air sparging. However, Johnson did not investigate the rate of oxygen diffusion into the contaminated zone. Wilson and Norris [2] developed mathematical models to calculate the rate of oxygen transport for bubble regime during in situ air sparging. Stright and

* Corresponding author. Tel.: +886 6 2757575x62827; fax: +886 6 2747378.
E-mail address: mctkuobe@mail.ncku.edu.tw (M.C.T. Kuo).

0304-3894/$ – see front matter © 2008 Elsevier B.V. All rights reserved.
doi:10.1016/j.jhazmat.2008.07.156

Gierke [3] developed a mathematical model to investigate the oxygen transport using the air-channel concept. Models developed by Wilson and Norris [2] and Stright and Gierke [3] were useful for performance evaluation and sensitivity analysis of oxygen dissolution during in situ air sparging. However, both models were not compared or verified directly with the experimental data obtained from oxygen dissolution tests. This paper combined both modeling and experimental approaches investigating the mass transfer rates of toluene-vapor and the transient concentrations in air and water before equilibrium is attained. The model simulations were compared against experimental data obtained from toluene-vapor dissolution tests. The objective of this paper is to develop a simple model to predict the dissolution transient behavior of gaseous substrates for an in situ sparging process using their chemical and physical properties, aquifer-media characteristics, and field operating conditions. In addition, experimental data obtained from toluene-vapor dissolution tests were used to verify the model predictions.

Elder et al. [18] developed an air-sparging model using the air-channel concept. There are similarities in mass transfer equations between air sparging and our dissolution processes. This paper extends Elder's method and applies the air-channel concept from air-sparging problems to dissolution problems.

This paper presents a simple means to predict the dissolution transient behavior of gaseous substrates for an in situ sparging process. The validity of simplified assumptions and model predictions are verified with toluene-vapor dissolution tests. This paper also illustrates an example application of the verified model in the field-scale to investigate the influence of the sparging depth on the dissolution efficiency.

2. Model development

The mechanisms of the gaseous substrates (or, toluene-vapor) dissolution through air injection are similar to the air sparging, however, the direction of mass transfer is reversed. Air-sparging models available in the literature [1–3,18–21] to predict mass removal from groundwater are helpful for this study to construct the gaseous substrates (or, toluene-vapor) dissolution model. Even though there are similarities in mass transfer equations, there are also significant differences between the air-sparging model and dissolution model. This paper presents a simple mathematical model to predict the dissolution process of gaseous substrates applying the air-channel concept [3,18,21].

The air-flow geometry occurring during air sparging depends on the grain size of aquifer-media. Based on laboratory observations [22–24], channel flow occurs in media with grain sizes smaller than 2 mm and bubble flow occurs in media with grain sizes greater than 2 mm. A chamber-flow geometry [25] was also observed in air sparging of very fine-grained sands (grain diameter <0.2 mm). The dissolution model using the air-channel concept developed in this study applies to coarse-sand and medium-sand aquifers.

Nomenclature

C_g	average vapor concentration of toluene in the air cell ($g\,m^{-3}$)
C_{gi}	the concentration of toluene-vapor in the injected air ($g\,m^{-3}$)
C_{LA}	aqueous concentrations at mean radius r_A from the centerline of the element ($g\,m^{-3}$)
C_{LB}	aqueous concentrations at mean radius r_B from the centerline of the element ($g\,m^{-3}$)
C_{Lb}	aqueous concentration in the bulk pore fluid located in the annular ring adjacent to the air cell ($g\,m^{-3}$)
d_c	air-channel diameter (m)
D_g	vapor diffusion coefficient ($m^2\,s^{-1}$)
D_L	aqueous diffusion coefficient ($m^2\,s^{-1}$)
D_w	sparging depth of well (m)
$E_{dissolution}$	dissolution efficiency (%)
k_g	mass transfer coefficient of gas film ($m\,s^{-1}$)
k_L	mass transfer coefficient of liquid film ($m\,s^{-1}$)
K_f	mass transfer coefficient for the liquid–vapor film at the interface of the air cell and pore liquid ($m\,s^{-1}$)
K_h	Henry's law constant
L	length of the air channel (m)
M	molecular weights (g)
$M_{dissolution}$	mass dissolved in the sparging tank (g)
n	porosity (fractional)
N_B	baseline neutron reading before air sparging
N_c	number of representative air channels in an entire plume
N_R	Reynolds number
N_{Sc}	Schmidt number
N_{Sh}	Sherwood number
N_{SS}	steady-state neutron reading during air sparging
P	pressure (atm)
Q	air flow rate of the sparging well ($m^3\,h^{-1}$)
Q_c	air flow rate per air channel ($m^3\,h^{-1}$)
R_i	radius of influence of the air plume (m)
r_A	radius distance from the center of annular ring A to air cell (m)
r_B	radius distance from the center of annular ring B to air cell (m)
S_a	air saturation (%)
S_c	spacing of a representative air channel at the watertable (m)
t	injection time (min)
t_a	exposure time of the liquid particle in contact with the gas (s)
T	temperature (K)
T_C	critical temperature (K)
V	molar volume at its normal boiling point ($cm^3\,g^{-1}\,mol^{-1}$)
V_C	critical molar volume (L)
V_g	air velocity in an air channel ($m\,s^{-1}$)
V_n	volume of the air cell in element n
ΔM_g	mass transferred from the air channel into the groundwater by dissolution (g)
ΔM_s	mass transferred in the aqueous phase between each set of adjacent annular rings in the soil annulus (g)
Δt	size of time step (s)
Δz	height of an element in the air channel (m)

Greek letters

Ψ_B	association parameter for solvent B (2.6 for water)
μ	viscosity of aqueous solution (cp)
μ_a	dynamic viscosity of air ($g\,s^{-1}\,m^{-1}$)
ρ_a	density of air ($g\,m^{-3}$)
τ	tortuosity

2.1. Conceptual model

Both field measurements [22,23,26] and our study indicate that air saturation and air channel density are highest near the sparging well and decreases radially away from the sparging well. Air channels appear in various diameters, lengths, and spacing inside the plume. Rather than calculating mass transfer for all air channels in the air plume, our model assumed that the dissolution of gaseous substrates could be calculated using the concept of a representative or an averaging air channel. The representative air channel has an air saturation, porosity, diameter, length, and spacing equals to the average properties of the entire air plume. Our model further assumed the representative air channel passing through $1/4(R_i)$ as recommended in the modeling of in situ air sparging [18,21]. The validity of simplified assumptions would be further checked by verifying model predictions with toluene-vapor dissolution tests. Air saturation, porosity, and air-channel diameter were measured in the dissolution tests for the average properties in the plume.

The left-hand side of Fig. 1 shows the conceptualized model for an in situ air plume with a radius of influence (R_i). It is assumed that an air plume consists of air channels extending from the sparging point of the injection well to the water table and the air channels are oriented symmetrically around the injection well. The right-hand side of Fig. 1 represents the mathematical model based on air-channel concept. A straight-line flow path is assumed for air channels and the real length of air channels could be adjusted using tortuosity. Fig. 2 also shows the representative air channel of length L is divided into a series of contiguous elements, each with an element height of Δz. Each element contains an air cell surrounded by a soil annulus. The soil annulus of each element is subdivided into four annular rings [18].

In our model, air is assumed to flow upward through a series of air cells and ground water is assumed to be stationary. Upward mass transfer through the air channel by advection mechanism is significantly larger than that through upper and lower edges of each soil annulus by diffusion mechanism. Upward mass transfer between elements is assumed to occur only in the vapor phase through the air channel. A no-flux boundary condition is imposed at the upper and lower edges of each soil annulus. A no-flux boundary is also assumed at the outer edge of the soil annulus because that edge represents a line of symmetry between the annulus and its neighbor. Sorption, biodegradation, and chemical reactions are ignored in our model.

2.2. Mathematical model of toluene-vapor dissolution

2.2.1. Mass transfer in an entire air plume

Toluene dissolved into an entire plume is estimated by multiplying mass dissolved from an average air channel by the number of channels in the plume. Elder's equations [18] to calculate the number and spacing of average air channels for an entire plume are summarized as follows. The number of representative air channels in an entire plume (N_c) is calculated as the quotient of the area of the air plume at the water table and the area of a circle with radius, $S_c/2$, surrounding a representative air channel at the water table as follows.

$$N_c = \frac{4R_i^2}{S_c^2} \tag{1}$$

where R_i is the radius of influence of the air plume (m); and S_c is the spacing of a representative air channel at the watertable (m). The spacing between adjacent representative air channels (S_c) as a function of the air saturation (S_a), air-channel diameter (d_c), and porosity (n) is written as follows [18].

$$S_c = \frac{d_c}{\sqrt{S_a n}} \tag{2}$$

The radius of influence (R_i) can be estimated from the following empirical function of airflow and depth of sparging point proposed by Elder [21].

$$R_i = 0.9 D_w^{0.93} [\log(0.588Q + 1)]^{0.5} \tag{3}$$

where D_w is the sparging depth of well (m) and Q is the air flow rate of the sparging well (m^3/h).

2.2.2. Mass transfer in a representative air channel

The mass transfer of toluene dissolution consists of two steps, i.e. (1) dissolution from the gas phase into the groundwater through the gas and liquid films [27,28], and (2) diffusion in the groundwater. The mass transferred from the air channel into the groundwater by dissolution during a time step (ΔM_g) is calculated for an element as follows.

$$\Delta M_g = \pi d_c \Delta z K_f (C_g - C_{Lb} K_h) \Delta t \tag{4}$$

where d_c is the diameter of the air channel (m); Δz is the height of an element in the air channel (m); K_f is the mass transfer coefficient for the liquid–vapor film at the interface of the air cell and pore liquid (m/s); K_h is the Henry's law constant of toluene, dimensionless; C_{Lb} is the aqueous concentration of toluene in the bulk pore fluid located in the annular ring adjacent to the air cell (g/m^3); C_g is the average vapor concentration of toluene in the air cell (mg/L); and Δt is the size of time step (s). The equilibrium toluene concentration in plume is governed by Henry's law. Positive mass transfer occurs when mass passes from the air cell into the soil annulus. The determination of sizes for time step and element height will be discussed at the end of this section. The coefficient K_f incorporates the resistance of the gas and liquid films (mass transfer coefficients k_g and k_L, respectively). Details of mass transfer equations for calculation of K_f, k_g and k_L are provided in Appendix A.

After computing the mass transferred from each air cell into the groundwater by dissolution (ΔM_g), the concentration in the annular ring adjacent to each air cell is then calculated to reflect the mass transferred into the groundwater by dissolution. Diffusive mass transfer in the aqueous phase between each set of adjacent annular rings in the soil annulus (ΔM_S) is calculated for a time step as follows.

$$\Delta M_S = \frac{2\pi D_L n (C_{LA} - C_{LB}) \Delta z \Delta t}{\ln(r_A/r_B)} \tag{5}$$

where C_{LA} and C_{LB} are the aqueous concentrations of toluene at mean radii r_A and r_B from the centerline of the element (g/m^3), respectively; D_L is the aqueous diffusion coefficient of toluene (m^2/s); n is the porosity, fraction; Δz is the height of the element (m); and Δt is the time step (s). Eqs. (4) and (5) are coupled at the first ring adjacent to the air cell. C_{LB} in Eq. (4) corresponds to C_{LA} in Eq. (5). Eq. (5) is an approximate solution to the diffusion equation and requires Δt to be small. In addition, Eq. (5) assumes that the aqueous concentration of toluene within each annular ring is constant for a time step. A marching solution employing time steps is used to approximate transient mass transfer of toluene. Aqueous diffusion commonly limits the toluene dissolution when air channels are widely spaced because aqueous diffusion coefficients are typically smaller than film mass transfer coefficients [29].

At a given time (t), mass transfer by dissolution from the air cell and by diffusion through the soil annulus during a time step (Δt) is calculated for all elements in a representative air channel using Eqs. (4) and (5). As gas moves up from the air cell of lower element

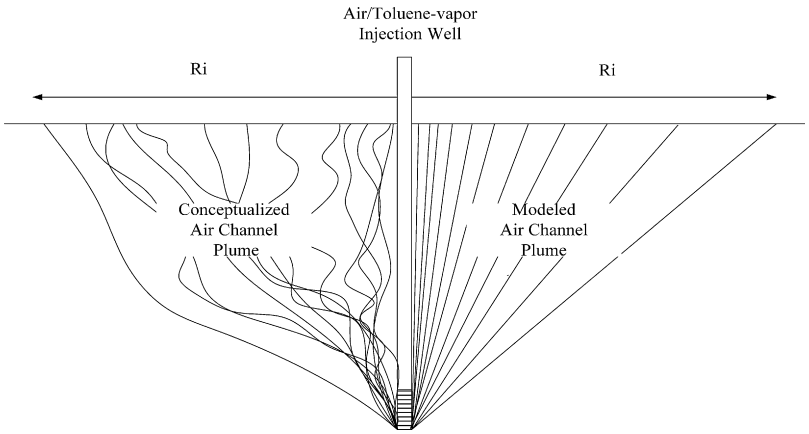

Fig. 1. Conceptualized and modeled air channels of air-sparging plume (adapted from Elder et al. [18]).

$n-1$ to the air cell of upper element n, the gas phase concentration decreases due to the dissolution of mass into groundwater. The gas phase concentrations entering into and leaving from the air cells of lower element $n-1$ and upper element n can be calculated by the mass balance equations as follows.

(1) Gas phase concentration entering into the air cell of lower element $n-1$

$$C_{\text{g in},n-1,t-2\Delta t} \tag{6}$$

(2) Gas phase concentration entering into the air cell of upper element n, or, leaving from the air cell of lower element $n-1$

$$C_{\text{g in},n,t-\Delta t}=C_{\text{g out},n-1,t-\Delta t}=C_{\text{g in},n-1,t-2\Delta t}-\frac{\Delta M_{g,n-1,t-\Delta t}}{V_{n-1}} \tag{7}$$

(3) Gas phase concentration leaving from the air cell of upper element n

$$C_{\text{g out},n,t}=C_{\text{g in},n,t-\Delta t}-\frac{\Delta M_{g,n,t}}{V_n} \tag{8}$$

where V_n is the volume of the air cell of upper element n; V_{n-1} is the volume of the air cell of lower element $n-1$; ΔM_g is the mass transferred from the air cell into the soil annulus; C_g is the gas phase concentration in the air cell; t is a given time; Δt is a time step.

To keep model computations stable, we used a beta ratio ($\beta<0.05$) to check the height of an element (Δz). The beta ratio is defined as a specified percentage of the mass β from the air cell transferred into the innermost annular ring of the soil element

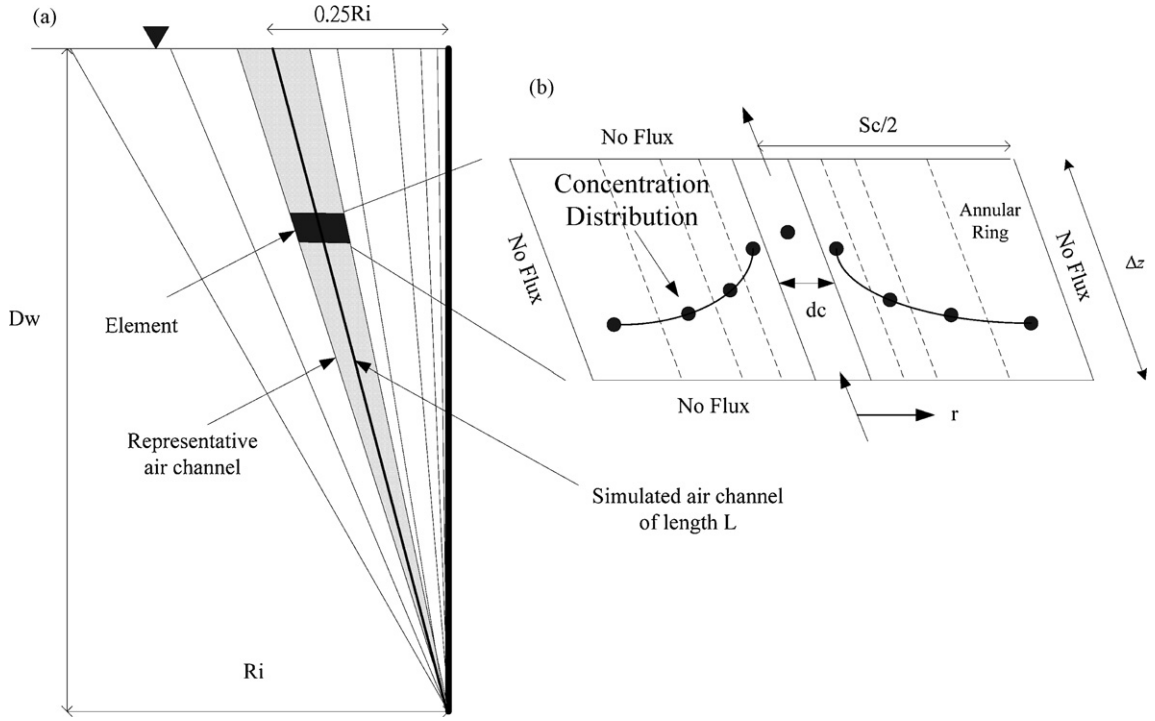

Fig. 2. Schematic diagrams showing (a) the representative air channel and (b) discrete element containing air cell and soil annulus (adapted from Elder et al. [18]).

during a time step Δt.

$$\beta = \frac{\pi^2 d_c^3 K_f C_g \Delta z^2}{C_g \pi \Delta z d_c^2 Q_c} \quad (9)$$

where flow rate per air channel (Q_c) is determined by dividing the air flow rate of the sparging well (Q) by the number of air channels (N_c) in the air plume, or,

$$Q_c = \frac{Q}{N_c} \quad (10)$$

With the size for element height (Δz) known, the size for time step (Δt) can be determined as follows.

$$\Delta t = \frac{\pi d_c^2 \Delta z}{4 Q_c} \quad (11)$$

For both the laboratory-scale and field-scale problems in this paper, a Δz value = 0.02 m is recommended for the height of an element in the air channel. It is also essential to verify that the height of an element (Δz) is sufficiently small to give accurate results of model computations. Details of choosing a Δz value = 0.02 m and the corresponding size for time step (Δt) are provided in Appendix B.

3. Materials and methods

3.1. Apparatus

Fig. 3 shows a schematic diagram showing venturi tube and sparging tank design used for the toluene-vapor dissolution tests. Toluene-vapor injection was accomplished through the use of venturi tube where the injected air vaporizes and carries toluene from a liquid-toluene reservoir located at the vena contracta of the venturi tube (Fig. 3a). The delivery design applies specifically to electron donors such as toluene which are in liquid state at ambient temperature and pressure [17].

The toluene-vapor dissolution tests were conducted to determine toluene dissolution efficiency with known properties of aquifer-media and measured operational conditions such as the injection time, the air flow rate, the concentration of toluene-vapor in injected air, the sparger depth, etc. Fig. 3b shows the schematic diagram of sparging tank design for the toluene-vapor dissolution tests. The mixture of air and toluene-vapor was injected through a sparging well into water contained in a sparging tank filled with coarse sand. The dimension of the sparging tank was 0.45 m × 0.65 m × 0.55 m in width, length, and depth, respectively. The porosity of the sparging tank was 0.35. The free water table was kept at 0.40 m above the bottom of the sparging tank. The sparging tank contained 40 L water.

The sparging well was located at the center of the sparging tank. The sparger was a 5 cm long screen located at the bottom of the sparging tank. An aluminum tube for neutron-probe access was installed in the sparging tank for measuring air saturation. A 40 cm long screen was placed at the bottom of the sparging tank for draining and sampling water. Sand thickness was 50 cm which is 10 cm higher than the water table for the purpose to observe water mounding phenomena and to measure the diameters of air channels. Mounding first developed during the transient expansion stage, then dissipated during the collapse stage, and was negligible at the steady state. The diameters of air channels were measured from the top-view photos taken at the steady state.

The coarse sand and tap water were placed in the sparging tank layer by layer at 5-cm thick a layer each time to avoid entrapment of air within the sand during placement. Coarse sand was glued to the walls of the sparging well and the neutron access tube to discourage preferential flow of air along the pipe walls.

3.2. Measurements of air saturation

A Troxler 4300 series depth moisture probe was used to measure air saturation. The neutron probe is estimated to have a measurement of radius of 15.2–20.3 cm (or, 6–8 in.) around the access pipes. Measurements were taken at 25 cm above the bottom of the sparging tank. A 30-s counting time was used for each measurement. The air saturation is calculated as follows [30].

$$S_a = \frac{(N_B - N_{SS}) \times 100}{N_B} \quad (12)$$

where S_a is the steady-state air saturation during air sparging (%); N_B and N_{SS} are the baseline neutron reading before air sparging and the steady-state neutron reading during air sparging, respectively.

3.3. Toluene-vapor dissolution tests

Toluene-vapor dissolution tests were conducted to determine the dissolution efficiency and to verify the model predictions. Six tests were conducted at two air flow rates (40 and 80 L/min) and at three injection times (5, 10, and 15 min). Toluene-vapor was injected with air after steady-state air channels were established. It took approximately 2 h air-injection time to achieve a steady-state condition when steady readings from neutron probe were attained. The concentration of toluene-vapor in the injected air was at 5.6 mg/L; and the sparging tank contained 40 L water.

To measure the total toluene mass dissolved in the sparging tank, 40 mL water samples for toluene analysis were immediately taken from the sampling valve at the bottom of the sparging tank at the end of each dissolution test. Water samples were collected at an interval of 2 L water drained. The toluene concentrations measured in the effluent samples were used to calculate the average toluene concentration in the sparging tank. The total toluene mass dissolved in the sparging tank was then calculated by multiplying the average toluene concentration with the water volume in the sparging tank. The dissolution efficiency of toluene-vapor can be determined as follows.

$$E_{dissolution} = \frac{M_{dissolution} \times 100}{(C_{gi} Q t)} \quad (13)$$

where $E_{dissolution}$ is the dissolution efficiency (%); $M_{dissolution}$ is the toluene mass dissolved in the sparging tank (g); C_{gi} is the concentration of toluene-vapor in the injected air (g/m^3); Q is the air flow rate of the sparging well (m^3/min); t is the injection time of gaseous substrates (min).

3.4. Toluene analysis

Toluene was measured using a gas chromatograph (HP 6890 GC) with a J&W Scientific DB1, 60 m, 0.32 mm i.d. capillary column, and mass selective detector (HP 5973 MSD). Zero-grade helium carrier gas flow rate was 25 mL/min at a head pressure of 4.24 psig. The temperatures of injector and detector were 200 and 265 °C, respectively. A purge and trap (Tekmar Velocity XPT with a Tekmar Purge Trap K) was used. Samples of 5 mL were added to sampling tubes and purged for 11 min at 35 °C. Desorption preheat was at 265 °C and desorption time was 4 min at 270 °C. The trap lines and valves were kept constant at 150 °C and the injection port was 265 °C. The detection limits for toluene was 1.1 μg/L.

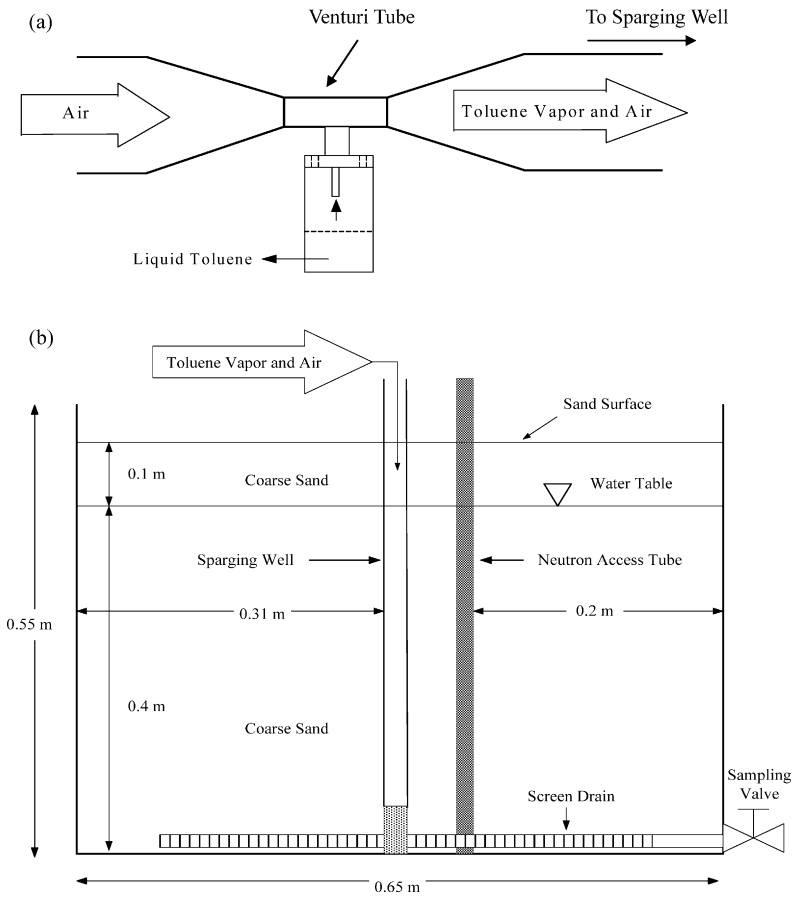

Fig. 3. Schematic diagrams showing (a) venturi tube and (b) sparging tank used for toluene-vapor dissolution tests.

4. Results and discussion

4.1. Air saturation and diameter of air channels

A neutron probe was used to measure changes in percent air saturation in the sparging tank during air sparging at three air flow rates (Q = 40, 60, and 80 L/min). Table 1 shows the measurement results of air saturation using the neutron moisture probe at steady-state conditions for three air flow rates (Q = 40, 60, and 80 L/min). As the air flow rate increases from 40 to 80 L/min, the air saturation increases from 9% to 16%. A neutron probe was also used by Acomb et al. [26] to measure changes in percent air saturation during air sparging in uniform sand. At air flow rates of 110–450 L/min, the percent air saturation ranged from about 30% to 50% near the sparging well.

From the grain size distribution curve for the coarse sand used in the sparging tank, the median particle size (D_{50}) and the uniformity coefficient (D_{60}/D_{10}) were 0.49 mm and 4, respectively. The air-flow geometry occurring during air sparging depends on the grain size of aquifer-media based on laboratory observations [22–24]. Air-flow geometry in saturated media of medium to coarse sand is expected to occur in discrete air channels.

Table 1
Measurements of air saturation using neutron moisture probe

Air flow rate (L/min)	Neutron counts in 30 s		Air saturation (%)
	Background	Steady state	Steady state
40	500	454	9.2
60	495	434	12.3
80	496	419	15.5

Fig. 4 shows the air-channel exits from a top view of the air-sparging tank after 120 min of air injection at 80 L/min. Fig. 5 shows the box-and-whisker plot of the data of air-channel diameter measured at the top of the air-sparging tank. On the right-hand side, Fig. 5 shows the median (50th percentile, 1.6 mm) as a center bar. The whiskers (1.0 and 2.4 mm) cover all but the most extreme values in the data set. The air-channel diameter remains unchanging at air flow rates of 40–80 L/min.

Fig. 4. A top-view of the air-sparging tank showing air-channel exits 120 min of air injection at 80 L/min (white circles: air-channel exits).

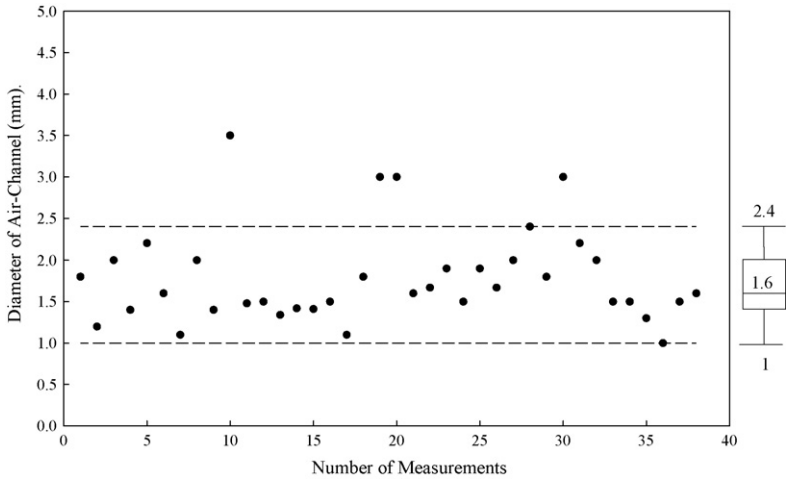

Fig. 5. Box-and-whisker plot for the data of air-channel diameter measured at the top of the air-sparging tank.

4.2. Model predictions and experimental verifications

Model calculations were made to predict average toluene concentration and total mass dissolved in plume for two air flow rates (40 and 80 L/min). Six dissolution tests were conducted for two air flow rates (40 and 80 L/min) and at three injection times (5, 10, and 15 min) to verify the model predictions.

The model calculates the mass transfer of toluene-vapor into groundwater using their chemical and physical properties, aquifer-media characteristics, and operational conditions of in situ sparging of gaseous substrates. The parameters used in the model calculations are listed in Table 2.

Fig. 6 shows the average toluene concentration in plume as a function of injection time for two air flow rates (Q = 40 and 80 L/min). The equilibrium toluene concentration in plume is governed by Henry's law. Given the concentration of toluene-vapor in injected air C_{gi} = 5.6 mg/L and the dimensionless Henry's law constant K_h = 0.344, the equilibrium toluene concentration in water is calculated as follows.

$$C_{Lb,eq} = \frac{C_{gi}}{K_h} = \frac{5.6}{0.344} = 16.3\ \text{mg/L}$$

The rate of toluene dissolution increases as the air saturation increases. For example, the injection time required to attain 95% of the equilibrium concentration of toluene is 150 and 350 min, respectively, for the air saturation of 16% and 9%. The cross points in Fig. 6 represent the injection time when 95% of the equilibrium concentration of toluene was attained in the plume.

Fig. 6 also shows that the dissolution rate of toluene-vapor decreases as the injection time increases. Fig. 6 indicates that the duration for each pulse of toluene-vapor injection is recommended not to exceed 25 min to take advantage of high dissolution rate. Therefore, we focused the model predictions and the dissolution tests in the early 25 min. Figs. 7 and 8 present the toluene mass dissolved in the sparging tank and the dissolution efficiency, respectively, for the early 25 min injection.

Fig. 7 compares the total mass of dissolved toluene calculated from the model with the experimental data measured in the dissolution tests. Six dissolution tests were conducted with toluene-vapor injected after steady-state air channels were established. Toluene-vapor was injected with air at a concentration of 5.6 mg/L for two air flow rates (40 and 80 L/min) and at three injection times (5, 10, and 15 min). For the six test conditions at 40 L/min, 5 min injection; 40 L/min, 10 min injection; 40 L/min, 15 min injection; 80 L/min, 5 min injection; 80 L/min, 10 min injection; and

Table 2
Input parameters used in the model simulations

Parameters	Parameter values	Value basis	Literature values	Refs.
Dissolution test conditions				
Injection time (min), t	5, 10, 15	m		
Sparger depth (m), D_w	0.4	m		
Air flow rate (L/min), Q	40, 80	m		
Concentration of toluene-vapor in injected air (mg/L), C_{gi}	5.6	m		
Toluene properties				
Density of air (g/m^3), ρ_a	1165	l		[36]
Vapor diffusion coefficient (m^2/s), D_g	7.81E−6	l		[27]
Aqueous diffusion coefficient (m^2/s), D_L	10.19E−10	l		[27,34]
Henry's law constant, K_h	0.344	l		[35]
Dynamic viscosity of air (g/s m), μ_a	1.864E−02	l		[36]
Aquifer properties				
Water temperature (°C), T	30	m		
Median particle size (mm), D_{50}	0.49	m		
Porosity, n	0.35	m		
Diameter of air channel (mm), d_c	1.6	m	0.5–11.5	[18,23]
Tortuosity, τ	0.9	l	0.56–1.0	[18,23]
Air saturation (%), S_a	9, 16	m	0.2–0.5	[26]

m = Measured; l = literature.

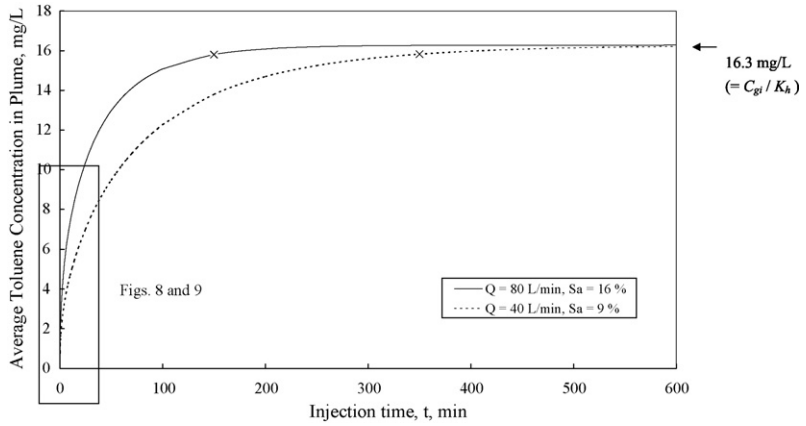

Fig. 6. Average toluene concentration in plume predicted as a function of injection time (C_{gi} = 5.6 mg/L, K_h = 0.344). The cross points represent the injection time when 95% of the equilibrium concentration of toluene was attained in the plume.

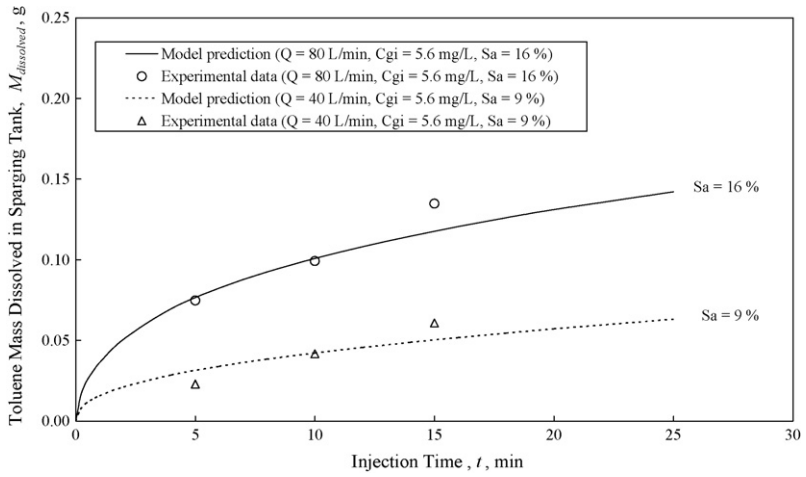

Fig. 7. Comparison of toluene mass dissolved in the sparging tank using model prediction and experimental data. The open circles and triangles represent data obtained from experiments in which toluene-vapor was injected after steady-state air channels were established.

80 L/min, 15 min injection, the average toluene concentrations dissolved in the sparging tank were measured at 0.573, 1.044, 1.599, 1.870, 2.480, and 3.371 mg/L, respectively. For a 40-L pore volume of water used in the dissolution tests, the corresponding total mass of toluene dissolved in the sparging tank were 0.0229, 0.0418, 0.0708, 0.0748, 0.0992, and 0.1348 g, respectively.

Fig. 7 shows that the total mass of dissolved toluene calculated from the model agrees well with the experimental data measured

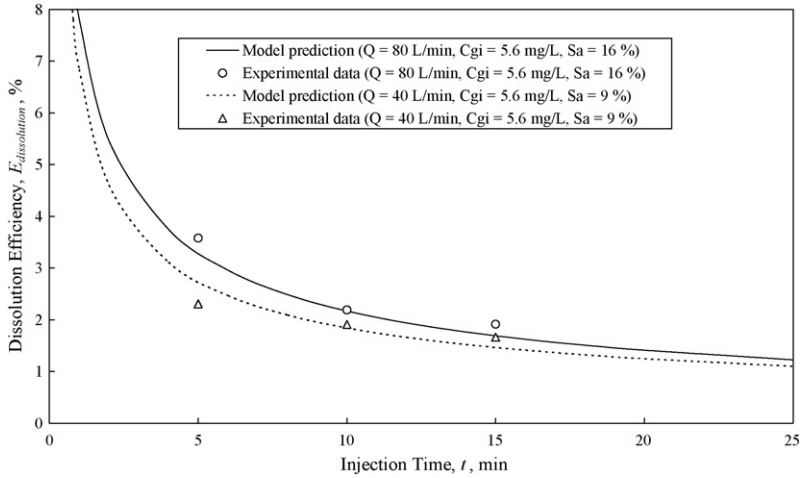

Fig. 8. Variation of toluene-vapor dissolution efficiency with injection time (Sparger depth, D_w = 0.4 m). The open circles and triangles represent data obtained from experiments in which toluene-vapor was injected after steady-state air channels were established.

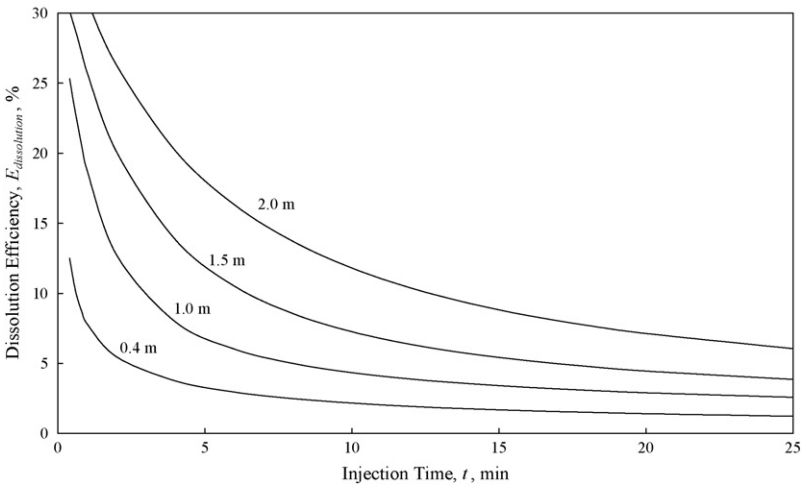

Fig. 9. Variation of toluene-vapor dissolution efficiency with injection time for Q = 80 L/min, C_{gi} = 5.6 mg/L with sparger depth (D_w) as parameter.

in the dissolution tests conducted at various injection times and rates. This implies that the model approach employing a representative air channel passing through 1/4(R_i) and other simplified assumptions made in the model development are valid. The verified model would be useful in designing the in situ sparging of gaseous substrates such as the injection time, the air flow rate, the concentration of toluene-vapor in injected air, the sparger depth, the dissolution efficiency, etc.

4.3. Dissolution efficiency of toluene-vapor

Fig. 8 compares the calculated dissolution efficiency of toluene-vapor versus injection time with the experimental data measured in the dissolution tests. For the six test conditions at 40 L/min, 5 min injection; 40 L/min, 10 min injection; 40 L/min, 15 min injection; 80 L/min, 5 min injection; 80 L/min, 10 min injection; and 80 L/min, 15 min injection, the dissolution efficiencies of toluene-vapor were measured at 2.1%, 1.9%, 1.7%, 3.6%, 2.2%, and 1.9%, respectively. Fig. 8 shows that the calculated dissolution efficiency of toluene-vapor agrees well with the experimental data measured in the dissolution tests conducted at various injection times and rates. Fig. 8 also shows that the dissolution efficiency of toluene-vapor at an air flow rate of 80 L/min is higher than that at an air flow rate of 40 L/min. This could be due to that the air saturation at an air flow rate of 80 L/min is higher than that at an air flow rate of 40 L/min.

4.4. Model predictions of toluene-vapor dissolution efficiency in the field-scale

The most often used values of flow rate and sparging depth for an in situ air sparging process range from 40 to 140 L/min and from 1.5 to 3 m, respectively [31]. The verified model was used to investigate the influence of the sparging depth on the dissolution efficiency for an in situ air sparging process.

The radius of influence (R_i) of the air plume can be estimated as follows [21].

$$R_i = 0.9 D_w^{0.93} [\log(0.588Q + 1)]^{0.5} \quad (3)$$

where D_w is the sparging depth of well (m); Q is the air flow rate of the sparging well (m^3/h). Assuming a conical shape for the air plume, the pore volume (PV) of the air plume can be estimated as follows.

$$\mathrm{PV} = \frac{n\pi R_i^2 D_w}{3} \quad (14)$$

where n is the porosity, fraction; R_i is the radius of influence (m); D_w is the sparging depth (m). At the steady state and a given air flow rate, the air saturation (S_a) of the air plume can be estimated for any sparging depth as follows.

$$(\mathrm{PV}) \times S_a = \text{constant} \quad (15)$$

At the air flow rate of 80 L/min, the radius of influence (R_i), the pore volume (PV), and the air saturation (S_a) of the air plume are 0.30, 0.70, 1.02, and 1.34 m, 13, 181, 576, and 1316 L, 16%, 1.2%, 0.4%, and 0.2% for the sparging depth at 0.4, 1.0, 1.5, and 2.0 m, respectively. The radius of influence (R_i) and the pore volume of the air plume (PV) increases and the air saturation of the air plume (S_a) decreases with the increase in the sparger depth.

Fig. 9 shows the variation of the toluene-vapor dissolution efficiency as a function of the injection time with the sparger depth (D_w) as parameter. The air flow rate and the concentration of toluene-vapor in injected air used for Fig. 9 are Q = 80 L/min and C_{gi} = 5.6 mg/L. The results given in Fig. 9 indicate that the dissolution efficiency of toluene-vapor increases with the increase in the sparger depth, as expected.

5. Conclusions

1. A mathematical model using the air-channel concept was developed and verified to calculate the dissolution efficiency of gaseous substrates in an unconfined aquifer using their chemical and physical properties, aquifer-media characteristics, and operating conditions of an in situ sparging process.
2. Toluene-vapor dissolution tests were conducted to determine the dissolution efficiency at two air flow rates (40 and 80 L/min) and at three injection times (5, 10, and 15 min). The dissolution efficiencies of toluene-vapor were measured at about 2.0%.
3. The calculated dissolution efficiency of toluene-vapor agrees well with the experimental data measured in the dissolution tests conducted at various injection times and rates.

Acknowledgements

Support by National Science Council of Taiwan (NSC 94-2211-E-006-029 and NSC 95-2221-E-006-170-MY3) is appreciated. We

thank Drs. C.R. Elder and C.H. Benson for helpful discussions and providing the source code of the air-sparging model. We also thank Mr. C.H. Lin for neutron-probe measurements; and Mr. C.Y. Su and Mr. H.L. Wu for field assistance in dissolution tests.

Appendix A. Mass transfer equations

This appendix summarizes the mass transfer equations for calculating K_f, k_g and k_L. The mass transfer coefficient (K_f) at the interface of the air cell and pore liquid incorporates the mass transfer coefficients k_g and k_L, of the gas and liquid films, respectively. Gas and liquid film resistance are combined to predict K_f [27].

$$K_f = \left[\frac{1}{k_g} + \frac{K_h}{k_L}\right]^{-1} \tag{A1}$$

The coefficient for gas film resistance (k_g) is estimated using the Sherwood number (N_{Sh}), which describes the ratio of mass transfer resistance across the gas film to resistance by molecular diffusion into the film. The Sherwood number (N_{Sh}) is often expressed as a function of the Reynolds number (N_R), which describes the dynamics of gas flow, and the Schmidt number (N_{Sc}), which describes the relative impact of diffusive to convective mass transfer. In laminar flow, average Sherwood number (N_{Sh}) for the uniform wall concentration case for the air channel is defined as follows [32].

$$N_{Sh} = \frac{k_g d_c}{D_g} = 1.615\left(\frac{d_c}{L}\right)^{1/3}(N_R N_{Sc})^{1/3} \tag{A2}$$

where L is the length of the air channel (m) and D_g is the diffusion coefficient of toluene-vapor (m^2/s). The toluene-vapor diffusion coefficient (D_g) can be estimated as follows [27].

$$D_g = \frac{0.01498T^{1.81}(1/M_A + 1/M_B)^{0.5}}{P(T_{CA}T_{CB})^{0.1405}(V_{CA}^{0.4} + V_{CB}^{0.4})^2} \tag{A3}$$

where T is the temperature (K); P is the pressure (atm); M_A and M_B are molecular weights of toluene and air, respectively; T_{CA} and T_{CB} are critical temperatures of toluene and air, respectively; V_{CA}, V_{CB} are the critical molar volumes of toluene and air, respectively. The Reynolds and Schmidt numbers (N_R and N_{Sc}) are defined as follows.

$$N_R = \frac{V_g d_c \rho_a}{\mu_a} = \frac{4Q_c\rho_a}{(\pi d_c \mu_a)} \tag{A4}$$

$$N_{Sc} = \frac{\mu_g}{(\rho_a D_g)} \tag{A5}$$

where V_g is the air velocity in an air channel (m/s); Q_c is the flow rate per air channel (m^3/min); μ_a is the dynamic viscosity of air (g/s m); and ρ_a is the density of air (g/m^3).

Penetration theory [28,32,33] is used to predict k_L because the liquid film is assumed to be stationary relative to the gas phase. The average k_L for the air channel is then obtained by integrating the flux over the time of exposure.

$$k_L = 2\sqrt{\frac{D_L}{\pi t_a}} \tag{A6}$$

where t_a is the exposure time of the liquid particle in contact with the gas; D_L is the aqueous diffusion coefficient (m^2/s). The aqueous diffusion coefficient (D_L) can be estimated as follows [27].

$$D_L = 7.4\times 10^{-8}\frac{(\Psi_B M_B)^{0.5}T}{\mu V_A^{0.6}} \tag{A7}$$

where M_B is the molecular weight of solvent B (18 for water); Ψ_B is the association parameter for solvent B (2.6 for water); T is the water temperature (K); μ is the viscosity of aqueous solution (cp);

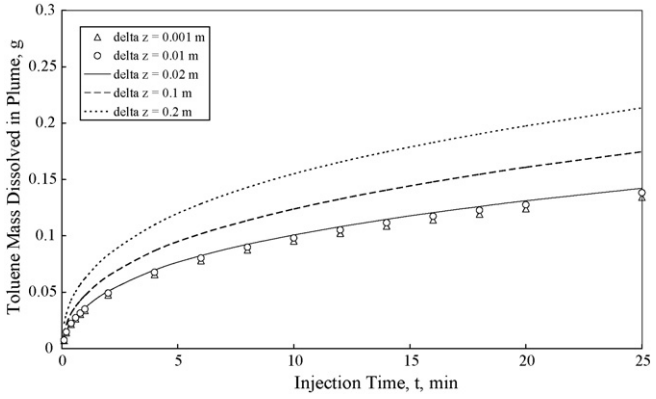

Fig. B1. Laboratory-scale model predictions of toluene mass dissolved in plume with Δz as parameter.

and V_A is the molar volume of toluene as liquid at its normal boiling point (cm^3/g mol). Substituting t_a in Eq. (A6) with $\pi d_c^2 L/4Q_c$ results as follows.

$$k_L = \frac{4}{\pi d_c}\sqrt{\frac{D_L Q_c}{L}} \tag{A8}$$

where L is the length of the representative air channel (m); Q_c is the flow rate per air channel (m^3/s).

Appendix B. Element height (Δz) and time step (Δt) recommended for model computations

This appendix describes the details for choosing a Δz value = 0.02 m and the corresponding size of time step (Δt) for model computations in both the laboratory-scale and field-scale problems.

Fig. B1 illustrates the laboratory-scale problem where D_w = 0.4 m, Q = 80 L/min, S_a = 16%, d_c = 1.6 mm, R_i = 0.3 m, K_f = 4.58E−5 m/s, S_c = 6.76E−3 m. Various values of Δz (0.2, 0.1, 0.02, 0.01, 0.001 m) were tried for model predictions. Fig. B1 shows laboratory-scale model predictions of toluene mass dissolved in plume with Δz as parameter. Table B1 presents variations of the beta ratio (β) and time step (Δt) with element height (Δz) for laboratory-scale model predictions. Fig. B1 indicates that it is essential to verify that the height of an element (Δz = 0.02 m) is sufficiently small to give accurate results of model computations. For Δz = 0.02 m, the corresponding size of time step (Δt) and the beta ratio (β) are 0.24 s and 2.7%, respectively.

Fig. B2 illustrates the field-scale problem where D_w = 2 m, Q = 80 L/min, S_a = 0.2%, d_c = 1.6 mm, R_i = 1.34 m, K_f = 4.11E−5 m/s, S_c = 6.05E−2 m. Various values of Δz (0.2, 0.1, 0.02, 0.01, 0.005 m) were tried for model predictions. Fig. B2 shows field-scale model predictions of toluene mass dissolved in plume with Δz as parameter. Table B2 presents variations of the beta ratio (β) and time step (Δt) with element height (Δz) for field-scale model predictions. Fig. B2 indicates that it is essential to verify that the height of an

Table B1
Variations of the beta ratio (β) and time step (Δt) with element height (Δz) for laboratory-scale model predictions

Δz (m)	β (%)	Δt (s)
0.001	0.14	0.012
0.01	1.4	0.12
0.02	2.7	0.24
0.1	14	1.2
0.2	27	2.4

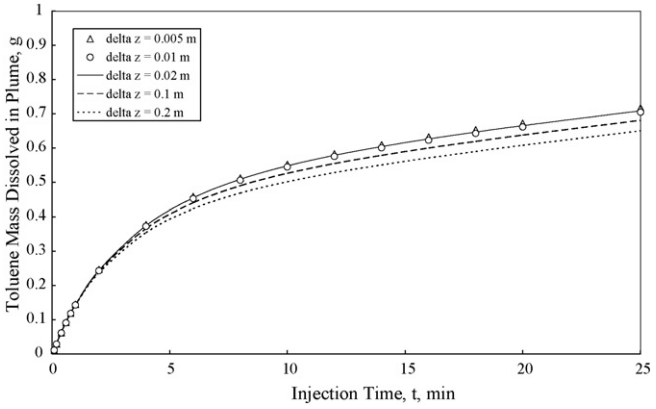

Fig. B2. Field-scale model predictions of toluene mass dissolved in plume with Δz as parameter.

Table B2
Variations of the beta ratio (β) and time step (Δt) with element height (Δz) for field-scale model predictions

Δz (m)	β (%)	Δt (s)
0.005	0.15	0.015
0.01	0.3	0.03
0.02	0.6	0.06
0.1	3	0.3
0.2	6	0.6

element ($\Delta z = 0.02$ m) is sufficiently small to give accurate results of model computations. For $\Delta z = 0.02$ m, the corresponding size of time step (Δt) and the beta ratio (β) are 0.06 s and 0.6%, respectively.

References

[1] P.C. Johnson, Assessment of the contributions of volatilization and biodegradation to in situ air sparging performance, Environ. Sci. Technol. 32 (2) (1998) 276–281.
[2] D.J. Wilson, R.D. Norris, Groundwater cleanup by in-situ sparging. XI. Engineered bioremediation with aeration curtains, Sep. Sci. Technol. 32 (16) (1997) 2569–2589.
[3] L.E. Stright, J.S. Gierke, Modeling of oxygen mass transfer during biosparging, in: Proceedings: In Situ and On-Site Bioremediation, The Fifth International Symposium, San Diego, CA, April, 1999, pp. 19–22.
[4] M.C. Marley, D.J. Hazebrouck, M.T. Walsh, The application of in situ air sparging as an innovative soils and ground water remediation technology, GWMR Spring (1992) 137–145.
[5] F.J. Brockman, W. Payne, D.J. Workman, A. Soong, S. Manley, T.C. Hazen, Effect of gaseous nitrogen and phosphorus injection on in situ bioremediation of a trichloroethylene-contaminated site, J. Hazard. Mater. 41 (1995) 287–298.
[6] J. Bae, L. Semprini, P.L. McCarty, Apparatus for down-well oxygen transfer into contaminated aquifers, J. Environ. Eng. 121 (8) (1995) 565–570.
[7] S.M. Pfifner, A.V. Palumbo, T.J. Phelps, T.C. Hazen, Effect of nutrient dosing on subsurface methanotrophic populations and trichloroethylene degradation, J. Ind. Microbiol. Biotechnol. 18 (1997) 204–212.
[8] B.J. Travis, N.D. Rosenburg, Modeling in situ bioremediation of TCE at Savannah River: effects of product toxicity and microbial interactions on TCE degradation., Environ. Sci. Technol. 31 (1997) 3093–3102.
[9] L. Semprini, Strategies for the aerobic co-metabolism of chlorinated solvents, Curr. Opin. Biotechnol. 8 (3) (1997) 296–308.
[10] A. Tovanabootr, L. Semprini, Comparison of TCE transformation abilities of methane- and propane-utilizing microorganisms, Bioremediation 2 (2) (1998) 105–124.
[11] A. Tovanabootr, L. Semprini, M.E. Dolan, M. Azizian, V.S. Magar, D. Debacker, A. Leeson, C.D. Kempisty, Cometabolic air sparging field demonstration with propane to remediate trichloroethene and *cis*-dichloroethene, in: A. Leeson, P.C. Johnson, R.E. Kinchee, L. Semprini, V.S. Magar (Eds.), The Sixth International In Situ and on site Bioremediation Symposium, Columbus, USA, Battelle Press, San Diego, CA, USA, 2001, pp. 145–153.
[12] J.M. Gosett, S.H. Zinder, Microbiological aspects relevant to natural attenuation of chlorinated ethenes, in: Proceedings from the Symposium on Natural Attenuation of Chlorinated Organics in Ground Water, EPA/540/R-96/509, Dallas, TX, 1996.
[13] C.J. Newell, R.T. Fisher, J. Hughes, Direct hydrogen addition for the in-situ biodegradation of chlorinated solvents, in: NGWA Petroleum Hydrocarbons Conference, Houston, TX, 1997.
[14] G.D. Hopkins, P.L. McCarty, Field evaluation of in situ aerobic cometabolism of trichloroethylene and three dichloroethylene isomers using phenol and toluene as the primary substrates, Environ. Sci. Technol. 29 (6) (1995) 1628–1637.
[15] P.L. McCarty, M.N. Goltz, G.D. Hopkins, M.E. Dolan, J.P. Allen, B.T. Kawakami, T.J. Carrothers, Full-scale evaluation of in situ cometabolic degradation of trichloroethylene in groundwater through toluene injection, Environ. Sci. Technol. 32 (1) (1998) 88–100.
[16] D.E. Ellis, E.J. Lutz, J.M. Odom, R.J. Buchanan, C.L. Bartlett, Bioaugmentation for accelerated in situ anaerobic bioremediation, Environ. Sci. Technol. 34 (11) (2000) 2254–2260.
[17] M.C.T. Kuo, K.F. Liang, Y.L. Han, K.C. Fan, Pilot studies for in-situ aerobic cometabolism of trichloroethylene using toluene-vapor as the primary substrate, Water Res. 38 (2004) 4125–4134.
[18] C. Elder, C. Benson, G. Eykholt, Modeling mass removal during in situ air sparging, J. Geotech. Geoenviron. Eng. 125 (11) (1999) 947–958.
[19] J.F. Pankow, R.L. Johnson, J.A. Cherry, Air sparging in gate wells in cutoff walls and trenches for control of plumes of volatile organic compounds (VOCs), Ground Water 31 (4) (1993) 654–663.
[20] A.J. Rabideau, J.M. Blayden, Analytical model for contaminant mass removal by air sparging, Groundwater Monit. Remed. 18 (4) (1998) 120–130.
[21] C. Elder, Modeling mass transfer during in situ air sparging, M.S. thesis, University of Wisconsin, Madison, Wisconsin, 1997.
[22] W. Ji, A. Dahmani, D. Ahlfeld, J. Lin, E. Hill, Laboratory study of air sparging: air flow visualization, Groundwater Monit. Remed. 13 (4) (1993) 115–126.
[23] C. Elder, C. Benson, Air channel formation, size, spacing, and tortuosity during in situ air sparging, Groundwater Monit. Remed. 65 (3) (1999) 171–181.
[24] J.W. Peterson, M.J. DeBoer, K.L. Lake, A laboratory simulation of toluene cleanup by air sparging of water-saturated sands, J. Hazard. Mater. 72 (2000) 167–178.
[25] J.W. Peterson, K.S. Murray, Y.I. Tulu, B.D. Peuler, D.A. Wilkens, Air-flow geometry in air sparging of fine-grained sands, Hydrogeol. J. 9 (2001) 168–176.
[26] L. Acomb, D. McKay, P. Currier, S. Berglund, T. Sherhart, C. Benediktsson, Neutron probe measurements of air saturation near an air sparging well, in: R. Hinchee, R. Miller, P. Johnson (Eds.), In Situ Aeration: Air Sparging, Bioventing and Related Remediation Processes, Battelle, Columbus, OH, 1995, pp. 47–61.
[27] W.A. McCabe, J.C. Smith, Unit Operations of Chemical Engineering, McGraw-Hill, Inc., 1976.
[28] R.E. Treybal, Mass-transfer Operations, McGraw-Hill, Inc., 1980.
[29] D. Ahlfeld, A. Dahmani, W. Ji, A conceptual model of field behavior of air sparging and its implications for application, Groundwater Monit. Remed. Fall (1994) 132–139.
[30] D.J. Mckay, L.J. Acomb, Neutron moisture probe measurements of fluid displacement during in situ air sparging, Groundwater Monit. Remed. Fall (1996) 86–94.
[31] M.C. Marley, C.J. Bruell, H.H. Hopkins, Air sparging technology: a practice update, in: R.E. Hinchee, R.N. Miller, P.C. Johnson (Eds.), In Situ Aeration: Air Sparging, Bioventing, and Related Remediation Processes, Battelle Press, Columbus, OH, 1995, pp. 31–38.
[32] A. Skelland, Diffusional Mass Transfer, Wiley, New York, 1974.
[33] R. Bird, W. Stewart, E. Lightfoot, Transport Phenomena, Wiley, New York, 1960.
[34] R.H. Perry, C.H. Chilton, Chemical Engineering's Handbook, McGraw-Hill, New York, 1974.
[35] D. Mackay, W.Y. Shiu, A critical review of Henry's law constants for chemicals of environmental interest, J. Phys. Chem. Ref. Data 10 (4) (1981) 1175–1199.
[36] H.D. Beggs, Gas Production Operations, Oil & Gas Consultants International, Inc., 1984.